Journal of Power Sources 196 (2011) 6603–6608

Contents lists available at ScienceDirect

Journal of Power Sources

journal homepage: www.elsevier.com/locate/jpowsour

Ag_2Se quantum-dot sensitized solar cells for full solar spectrum light harvesting

Auttasit Tubtimtae [a], Ming-Way Lee [a,*], Gou-Jen Wang [b]

[a] Institute of Nanoscience and Department of Physics, National Chung Hsing University, Taichung, 402, Taiwan
[b] Department of Mechanical Engineering and Institute of Biomedical Engineering, National Chung Hsing University, Taichung, 402, Taiwan

ARTICLE INFO

Article history:
Received 5 January 2011
Received in revised form 23 February 2011
Accepted 28 March 2011
Available online 6 April 2011

Keywords:
Silver selenide
Quantum dot
Solar cell
Successive ionic layer adsorption and reaction deposition

ABSTRACT

We report on the photovoltaic performance of Ag_2Se quantum-dot (QD) sensitized solar cells. The QDs are grown by the successive ionic layer adsorption and reaction process. The external quantum efficiency (EQE) spectrum of the assembled cells covers the entire solar power spectrum of 350–2500 nm with an average EQE of ~80% in the short-wavelength region (350–800 nm) and 56% over the entire solar spectrum. The effective photovoltaic range is ~7–14 times broader than that of the cadmium calcogenide system—CdS and CdSe. The photocurrent that Ag_2Se generates is four times higher than that of N3 dye. The best solar cell yields power conversion efficiencies of 1.76% and 3.12% under 99.4% and 9.7% sun, respectively. The results show that Ag_2Se QDs can be used as a highly efficient broadband sensitizer for solar cells.

1. Introduction

Solar cells are a crucial technology for solving the problems of high petroleum prices and global warming. Currently, the most widely used solar cells are silicon-based photovoltaic devices, but their high cost remains a problem. Recently, dye-sensitized solar cells (DSCs) have been emerging as a low-cost alternative photovoltaic source. The key components of a DSC include a photoelectrode, an electrolyte and a counterelectrode. The photoelectrode consists of a dye-coated TiO_2 film sintered to fluorine-doped tin oxide (FTO) glass. The nanoporous TiO_2 nanoparticles greatly increase the surface area for dye chemisorptions, resulting in enhanced light absorption. The best power conversion efficiency achieved by a DSC is ~11% [1]. The most commonly used organic dyes, N3 and N719, have large optical absorption coefficients in the visible range (400–700 nm), but small absorption coefficients in the infrared (IR). However, the solar spectrum covers the range of 0.3–2.5 μm, with ~70% of the photon flux being distributed beyond 700 nm. In other words, the dye wastes 70% of the solar photon flux. To improve efficiency, one needs to find new sensitizers with a broadband photoresponse, especially in the IR region. A successful option for broadband sensitizers is semiconductor (extremely thin layer) absorbers [2,3]. Semiconductor quantum dots (QDs) have also been used as sensitizers. QDs have several advantages over organic dye sensitizers such as having tunable absorption bands [4], high extinction coefficients [5], and multiple electron–hole pair generation [6]. The most extensively studied QD sensitizers are the cadmium chalcogenide systems: CdS and CdSe [7,8]. The lead chalcogenide compounds PbS and PbSe have also been explored [9,10].

We recently reported on a new QD sensitizer in the silver chalcogenide system Ag_2S, which has a broadband response in the spectral region of 0.3–1.1 μm and a respectable power conversion efficiency [11]. Another system of this family, namely Ag_2Se, is also an interesting candidate for broadband sensitizers. Ag_2Se has a very small energy gap (E_g ~0.07–0.15 eV, 300 K) [12]. It is also the only stable composition that occurs in the phase diagram of the Ag–Se system [13]. Ag_2Se nanoparticles have been synthesized by various methods [14,15].

In this work we investigate the photovoltaic properties of solar cells sensitized with Ag_2Se QDs. The dependences of the photovoltaic parameters on the number of SILAR cycles, passivation coating, and light intensity are studied. The external quantum efficiency (EQE) spectra reveal a photovoltaic range covering the full solar spectrum with high EQE values.

2. Experimental

Nanoporous TiO_2 films were prepared by spreading a TiO_2 paste (Dyesol DSL-18NR-T, particle size ~20 nm) onto an FTO glass substrate (15 Ω sq^{-1}) utilizing the procedure described previously [11]. Prior to the TiO_2 coating, the FTO glass was treated with a spin-coated titanium isopropoxide (Ti-iP) ethanol solution (0.2 M), then heated at 450 °C for 30 min. This treatment reduced the recombination of the photoelectrons at the FTO/TiO_2 interface. The thickness

* Corresponding author. Tel.: +886 4 22852783; fax: +886 4 22862534.
E-mail address: mwl@phys.nchu.edu.tw (M.-W. Lee).

0378-7753/$ – see front matter © 2011 Elsevier B.V. All rights reserved.
doi:10.1016/j.jpowsour.2011.03.074

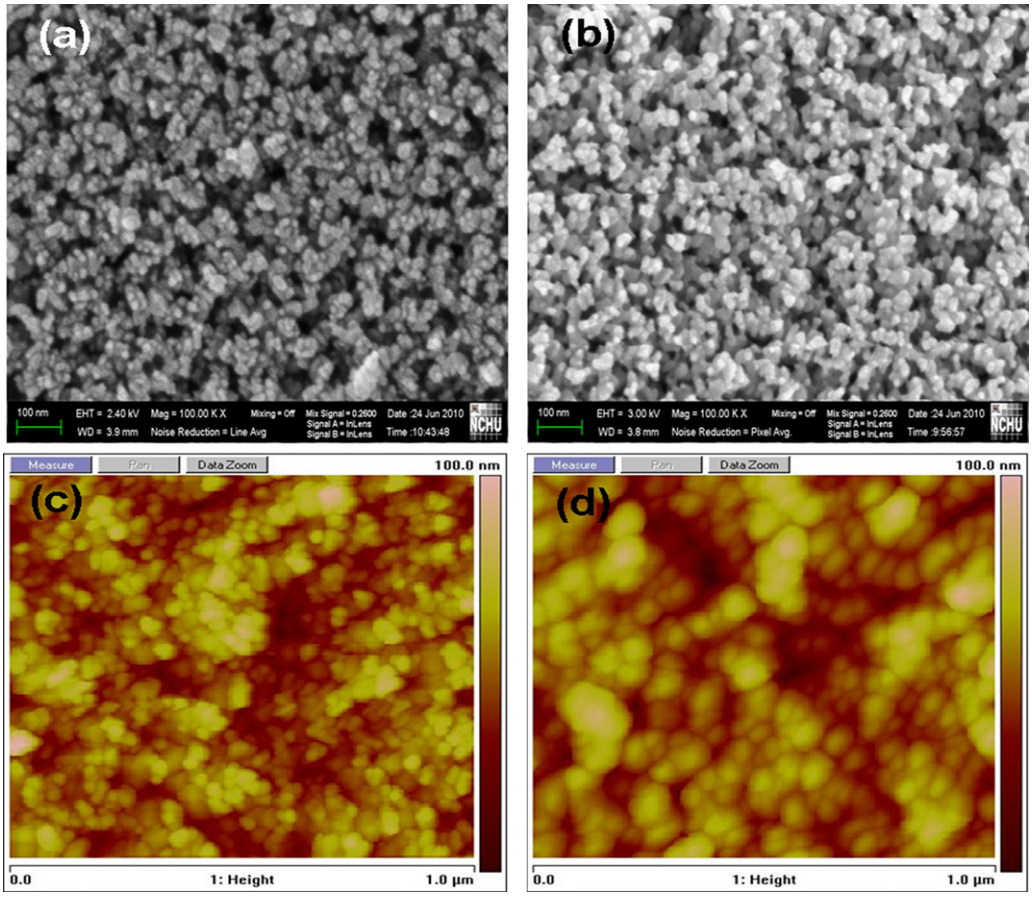

Fig. 1. FESEM micrographs of (a) uncoated, (b) $Ag_2Se(4)$-QDs-coated TiO_2 films. AFM micrographs of (c) uncoated, (d) $Ag_2Se(4)$-coated TiO_2 films.

of the TiO_2 film, determined from cross-sectional scanning electron microscopic (SEM) images, was ~10–12 μm. Finally, a 3 μm-thick TiO_2 scattering layer (size ~400 nm) was coated on the top of the film.

Ag_2Se QDs were synthesized using the successive ionic layer adsorption and reaction (SILAR) process [16]. The Ag^+ source was an $AgNO_3$ ethanol solution and the Se^{-2} source was a Na_2SeSO_3 aqueous solution, prepared by refluxing 0.3 M of Se in an aqueous solution of 0.6 M Na_2SO_3. A TiO_2 electrode was first dipped into the 0.1 M $AgNO_3$ solution at 25 °C for 1 min, rinsed with ethanol, and then dipped into the Na_2SeSO_3 solution at 50 °C for 1 h. The two-step dipping procedure comprises one SILAR cycle. Samples which went through n SILAR cycles are referred to as $Ag_2Se(n)$. The morphologies of the QDs were examined using atomic force microscopy (AFM, DI 3100 Veeco), field-emission scanning electron microscopy (FESEM, ZEISS Ultra plus) and transmission electron microscopy (TEM, JEOL-JEM 2010).

To further reduce the recombination of photoelectrons, a thin ZnS layer was coated onto the QD-loaded TiO_2 electrode by dipping the electrode into a 0.1 M $Zn(NO_3)_2$ ethanol solution for 1 min, then into a 0.1 M Na_2S methanol solution for 1 min. The ZnS coating reduces the recombination at the surface between the QDs and the electrolyte.

After the Ag_2Se-QD coating was completed, the TiO_2 electrode was assembled by sandwiching with a Pt-counterelectrode (preparation described in Ref. [11]) before being sealed with a 190 μm-thick parafilm spacer. Two types of electrolytes, polyiodide and polysulfide, were used in this work. The iodide/triiodide (I^-/I_3^-) electrolyte consisted of 0.05 M I_2, 0.1 M LiI, 1.0 M 4-tert-butylpyridine and 0.6 M 1-propyl-2,3-dimethylimidazolium iodide II in 3-methoxypropionitrile. The polysulfide electrolyte consisted of 0.5 M Na_2S, 2 M S, 0.2 M KCl and 0.5 M NaOH in methanol/water (7:3 by volume). To assure that the QDs do not dissolve in the I^-/I_3^- electrolyte, we performed tests on two kinds of QDs: Ag_2S and Ag_2Se. The experiment revealed that Ag_2Se QDs were stable after 30 min. In contrast, Ag_2S QDs dissolved instantly in I^-/I_3^- (see supplementary information).

The absorption spectra of the Ag_2Se QDs were measured using a Hitachi 2800A spectrophotometer. A FTIR interferometer (Perkin Elmer spectrum-1) was used to measure the spectra in the IR region of 2.5–25 μm. The current–voltage (I–V) curves were recorded with a Keithley 2400 source meter with an Oriel 150 W Xe lamp. An Oriel band pass filter simulated the AM 1.5 spectrum. The active area of the cell, defined by a metal mask, was 0.35 cm × 0.35 cm. The external quantum efficiency (EQE) spectra were recorded using an Acton monochromator with a 250 W tungsten-halogen lamp. Three power meters were used for different spectral ranges: a calibrated Si detector (Newport 1830-C, 350–1100 nm), a calibrated Ge detector (Thorlab PM100D, 1000–1800 nm) and a broadband thermal power meter (Thorlab S302A, 1800–2500 nm). The light intensity was varied by placing a metal grid in the light path. For each experimental condition, a batch of 3–4 samples were prepared and measured. The variations in efficiency were found to be ~10% for samples from the same batch. The whole experiment was repeated three times to ensure the consistency of the experimental data.

3. Results and discussion

Fig. 1 shows FESEM and AFM images of TiO_2 electrodes before and after QD coating with four SILAR cycles. The bare TiO_2 nanopar-

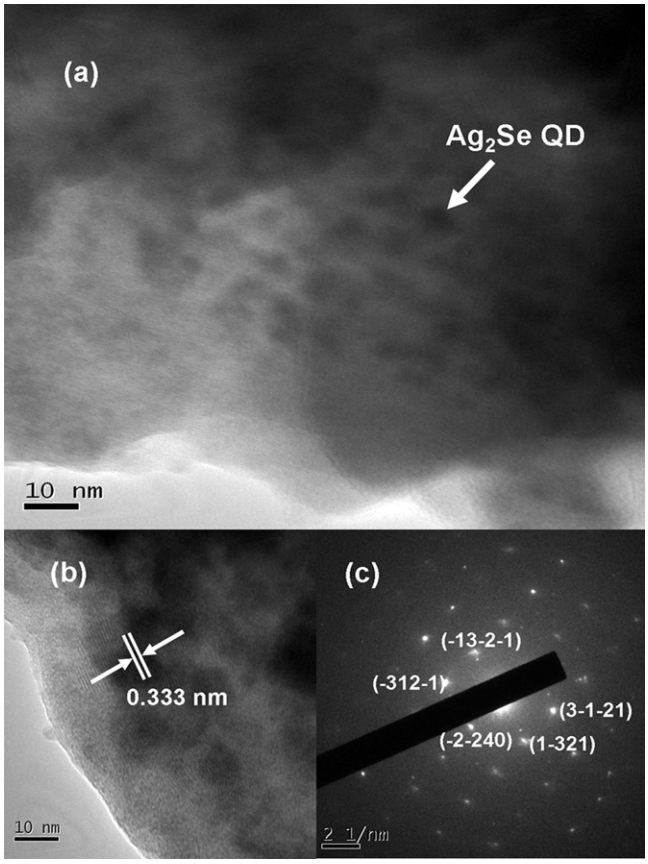

Fig. 2. TEM micrograph of (a) $Ag_2Se(4)$-QDs-coated TiO_2 film, (b) lattice fringes and (c) diffraction pattern of an individual QD.

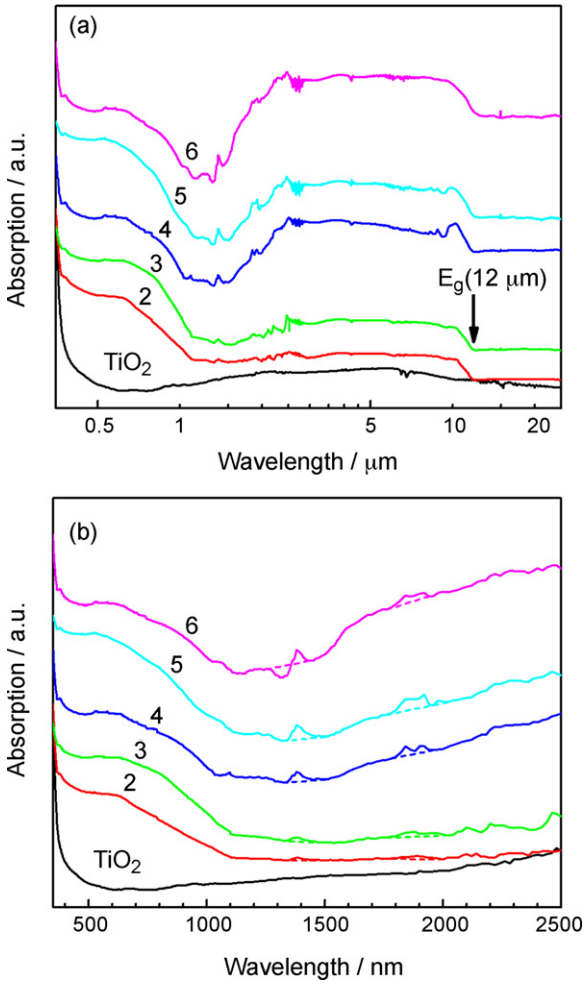

Fig. 3. (a) Optical absorption spectra of TiO_2 electrodes coated with various Ag_2Se QDs over the wide spectral range of 0.35–25 μm. The spectra are offset for clarity. (b) Absorption spectra for the solar spectra range of 350–2500 nm. The labels next to the curves denote the number SILAR cycles.

ticles (Fig. 1(a)) had an average diameter of ~15 nm and were aggregated into clusters of ~50 nm in diameter. After QD coating (Fig. 1(b)), a layer of film can be seen to cover the surface of the TiO_2 particles. The AFM images in Fig. 1(c) and (d) shows that the surface of the TiO_2 film became rougher after QD coating. The grain size also increased significantly. It was not possible to discern individual QDs from these images under the resolutions of the AFM and SEM. Fig. 2(a) shows a transmission electron microscope (TEM) image of the $Ag_2Se(4)$ sample. Many QDs can be seen to deposit randomly over the TiO_2 surface. The QDs are well separated and no aggregation is observed. The QDs have diameters in the range of 4–5 nm. Fig. 2(b) shows clear lattice fringes of a QD, indicating the high-quality crystalline structure of the QD. The fringe spacing is 0.333 nm, which corresponds to the (1 1 1) lattice plane. Fig. 2(c) shows a HRTEM microdiffraction rhombus pattern of an individual QD viewed along the [0 0 1] axis. Analysis of the diffraction pattern reveals an orthorhombic structure with the space group $P2_12_12_1$ (19) and lattice constants $a = 0.433$ nm, $b = 0.706$ nm and $c = 0.776$ nm (JCPDS no. 71–2410 standard) [17].

Fig. 3(a) shows the optical absorption spectra of Ag_2Se QD-loaded TiO_2 electrodes with various SILAR cycles n over the wide range of 0.35–25 μm. The spectra exhibit two broad peaks: the first in the short-wavelength (SW) region (400–1000 nm), the second in the long-wavelength (LW) region (1.5–12 μm). An absorption onset can be clearly identified at $\lambda = 12$ μm, which gives an energy gap of $E_g = 0.10$ eV. Fig. 3(b) shows the enlarged spectra over the solar spectral range of 350–2500 nm. Initially, a strong, broad band appears in the SW region of 400–1000 nm. In addition, a second, very broad absorption band starts to appear in the LW region of 1100–2500 nm for $n \geq 3$. The intensities of the two absorption peaks both increase with the SILAR cycle n. The two absorption peaks can be attributed to the various excitonic excitations associated with the band structure of Ag_2Se. The increasing absorption indicates that an increasing number of QDs are deposited on the TiO_2 electrodes as n is increased. The peak near 350 nm is due to the fundamental absorption edge of TiO_2.

Fig. 4 shows the photocurrent–voltage (I–V) curves of Ag_2Se QDs-sensitized solar cells with various SILAR cycles. Table 1 summarizes the photovoltaic parameters. Samples nos. 1–5 were treated with Ti-iP prior to TiO_2 coating and the electrolyte was the I^-/I_3^- redox couple. Initially, the short-circuit current density J_{sc} and the power conversion efficiency η increased with n. Optimal values of $J_{sc} = 27.2$ mA cm^{-2} and $\eta = 1.57\%$ were obtained at $n = 4$.

Table 1
Photoelectrochemical performance of Ag_2Se-QD sensitized solar cells with different SILAR cycles. Samples 1–5 were treated with a Ti-iP solution prior to TiO_2 coating. Electrolyte: sample nos. 1–6: I^-/I_3^- redox couple; no. 7: polysulfide.

Sample no.	Electrodes	J_{sc} (mA cm^{-2})	V_{oc} (V)	FF (%)	η (%)
1	$Ag_2Se(2)$	9.28	0.29	27.5	0.74
2	$Ag_2Se(3)$	17.3	0.26	22.3	1.01
3	$Ag_2Se(4)$	27.2	0.26	22.3	1.57
4	$Ag_2Se(5)$	24.4	0.26	21.6	1.37
5	$Ag_2Se(4)$/ZnS	28.5	0.27	23.8	1.76
6	$Ag_2Se(4)$/no Ti-iP	18.3	0.28	21.1	1.04
7	$Ag_2Se(4)$/ZnS – polysulfide	33.3	0.15	24.3	1.21

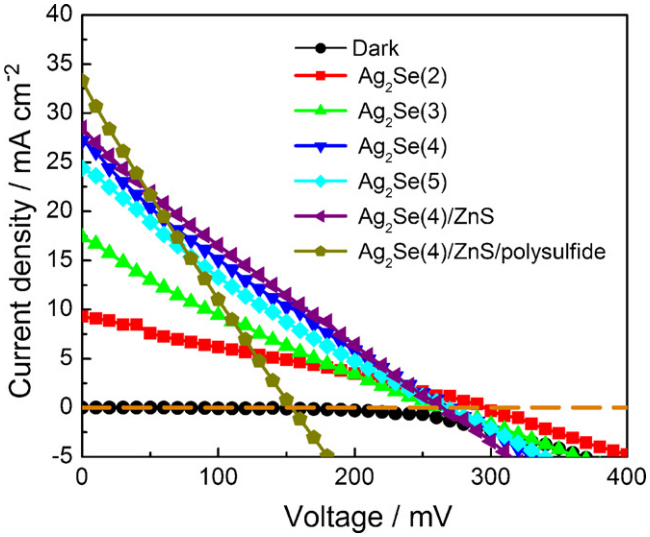

Fig. 4. Current–voltage curves of Ag_2Se DSCs processed with various SILAR cycles.

When $n \geq 5$, J_{sc} and η started to decrease again. The results indicate that J_{sc} and η increased with n (i.e., the amount of QDs deposited on TiO_2). However, when $n \geq 5$, overloading of QDs reduced the pore spaces in the electrode. This impeded the flow of electrolyte, resulting in smaller J_{sc} and η. The open-circuit voltage V_{oc} is ~0.26 V, and is independent of n. We also investigated the effects of the ZnS and Ti-iP coatings on cell performance. As can be seen in Table 1, the η of the optimal sample (no. 3) increased from 1.57 to 1.76% after the application of the ZnS coating (sample no. 5). In contrast, the sample without the Ti-iP coating (sample no. 6) had a η = 1.04%, significantly lower than the 1.57% of sample no. 3. The results show that ZnS and Ti-iP coatings are effective in enhancing the cell performance. We also studied the performance of cells using the polysulfide electrolyte. The $Ag_2Se(4)$/ZnS cell (sample no. 7) using a polysulfide electrolyte had a lower V_{oc} (0.15 V) and a lower η of 1.21%, ~30% lower than the 1.76% from sample no. 5 using the I^-/I_3^- electrolyte. This finding is consistent with the report that a polysulfide electrolyte produces a lower V_{oc} than the I^-/I_3^- electrolyte [18].

Fig. 5 displays the EQE spectra for the $Ag_2Se(4)$ samples with various passivation treatments over the range of 350–2500 nm.

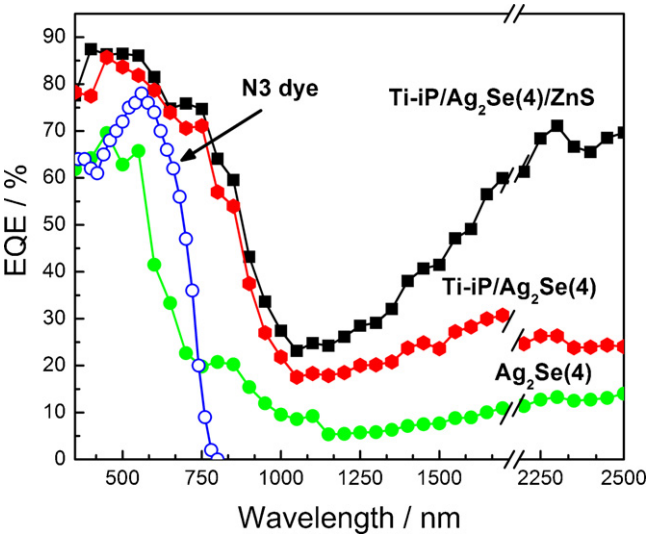

Fig. 5. External quantum efficiency spectra of $Ag_2Se(4)$ QD-DSCs with ZnS and Ti-iP coatings. For comparison, the spectrum of N3 dye (as in Ref. [20]) is also shown.

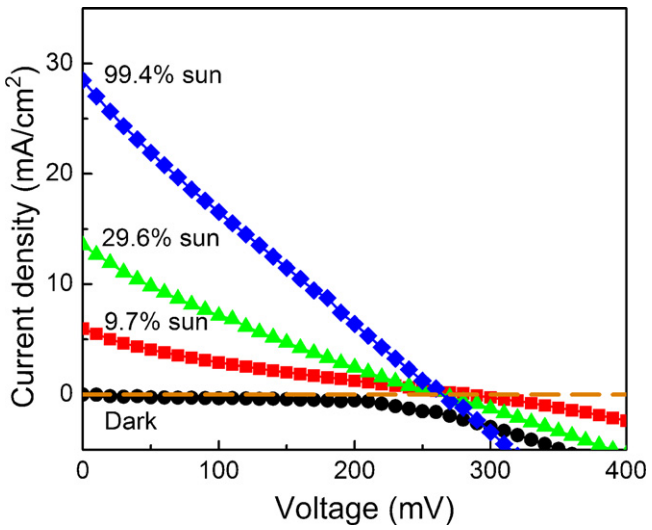

Fig. 6. Current–voltage curves under various sun intensities.

The EQE spectrum of the $Ag_2Se(4)$ sample without any passivation treatment exhibits large values of ~60–70% in the SW range (350–600 nm). At λ = 550 nm, the EQE starts to decrease rapidly with increasing λ, reaching a minimum at $\lambda \sim 1100$ nm, after which it increases gradually with λ again until λ = 2500 nm. The EQE spectrum of the $Ag_2Se(4)$ sample pretreated with Ti-iP exhibits significant enhancement over the entire spectral range. The EQE increases to 74–86% in the SW region (350–625 nm). In addition, the part of the wavelength where EQE decreases rapidly has shifted from 550 nm to 800 nm, which greatly increases the range of light harvesting. The EQE of the sample treated with both Ti-iP and ZnS coatings exhibited further enhancement over the Ti-iP/$Ag_2Se(4)$ sample. The best EQE spectrum exhibited two broad, strong bands: the first in the SW region (350–1000 nm), the second in the LW region (1000–2500 nm). The shape of the EQE spectrum was similar to that of the absorption spectrum shown in Fig. 3(b). The best EQE spectrum has the following average EQE values: (1) 80% in the SW range (350–800 nm); (2) 67% in the LW end of the spectrum (2200–2500 nm); (3) 56% over the entire spectrum (350–2500 nm).

Fig. 6 shows the I–V curves of the $Ag_2Se(4)$ samples under various light intensities P_{in}. Table 2 lists the photovoltaic parameters. The η increases as P_{in} is reduced. At 9.7% sun, η = 3.12%, significantly larger than the η (1.76%) at 99.4% sun.

The most important result of this work is the attainment of a broad EQE spectrum with large EQE values. The spectrum covers the entire solar spectral range of 350–2500 nm, giving an effective EQE range of 2150 nm. This means that Ag_2Se can use the full solar spectrum to generate photoelectrons. In contrast, the most extensively studied QD-systems – the cadmium chalcogenides – have the following ranges: CdS (spectral range: 400–550 nm, effective range ~150 nm) and CdSe (spectral range: 400–700 nm, effective range ~300 nm) [19]. The effective spectral range of Ag_2Se is ~7–14 times broader than that of the CdS/CdSe systems. For N3 dye, the spectral range is 350–700 nm and the effective range is 350 nm [20]. The effective spectral range of Ag_2Se is ~6 times broader than that of N3 dye.

Table 2
Photovoltaic parameters of $Ag_2Se(4)$-QD solar cells under various sun intensities. The electrodes were treated with Ti-iP and ZnS coatings.

	J_{sc} (mA cm^{-2})	V_{oc} (V)	FF (%)	η (%)
9.7% sun	5.97	0.28	18.2	3.12
29.6% sun	13.5	0.26	21.3	2.52
99.4% sun	28.5	0.27	23.8	1.76

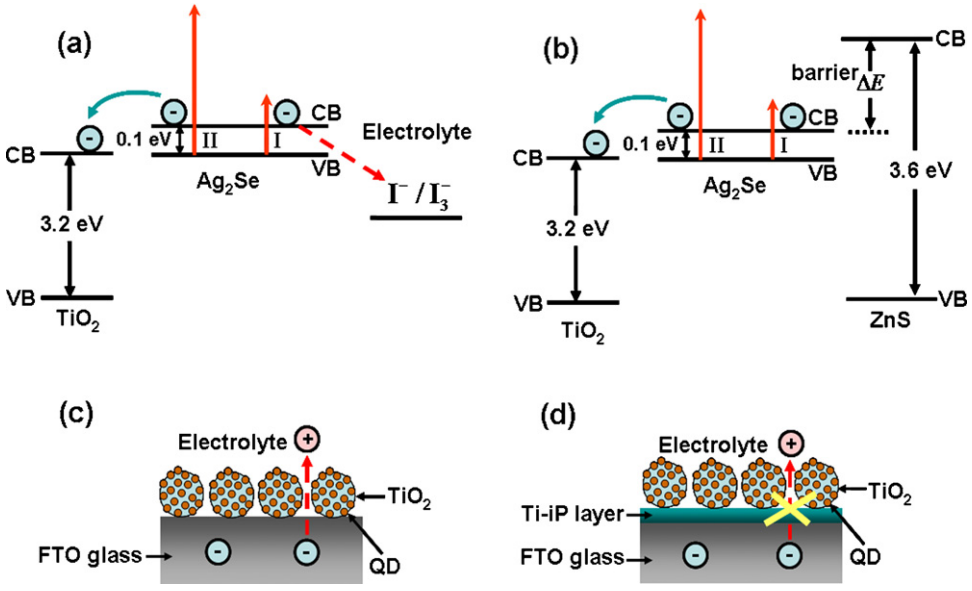

Fig. 7. Schematic energy-level diagrams of the Ag_2Se QD-DSC (a) before, (b) after the ZnS coating. Diagrams (c) and (d) show the reduced recombination of photoelectrons after the Ti-iP coating. The red-dash lines denote the route for recombination.

The total photocurrent density J_{ph} that a solar cell generates is given by:

$$J_{ph} = \int \Phi(\lambda)\mathrm{EQE}(\lambda)d\lambda$$

where $\Phi(\lambda)$ is the solar photon flux, which can be found in the literature. Our calculation reveals that the best EQE spectrum in Fig. 5 can produce $J_{ph} \sim 42\ \mathrm{mA\,cm^{-2}}$ (the maximum J_{ph} that a perfect solar cell can produce is $\sim 69\ \mathrm{mA\,cm^{-2}}$). We also compared the J_{ph} of Ag_2Se with N3 dye and found $J_{ph}(Ag_2Se)/J_{ph}(N3) = 3.6$, indicating that Ag_2Se can produce nearly four times the J_{ph} that N3 dye can.

The three EQE spectra in Fig. 5 indicate that the Ti-iP and ZnS coatings are effective in reducing the photoelectron recombination in Ag_2Se, leading to significantly enhanced EQE. However, the enhancement exhibits very distinct wavelength dependences for various coatings. The Ti-iP coating produces EQE enhancement over the whole spectrum (350–2500 nm). In contrast, the ZnS coating produces enhancement only in the LW region (1100–2500 nm); no enhancement is seen in the SW region. The phenomena can be explained by the energy band diagram shown in Fig. 7. In the DSC without ZnS coating, electrons are excited by photons from the valence band (VB) to the conduction band (CB) of Ag_2Se. Because the CB level is higher than the redox potential of the electrolyte, the photoelectrons can recombine with holes in the I^-/I_3^- electrolyte (Fig. 7(a)). For the sample with ZnS coating, a barrier with a height of $\Delta E = E_{CB}(ZnS) - E_{CB}(Ag_2Se)$ is formed at the Ag_2Se/ZnS interface (Fig. 7(b)). Electrons in the CB of Ag_2Se having energies below ΔE (red arrow I. Fig. 7(b)) are blocked from recombination by the barrier whereas electrons having energies above ΔE (red arrow II) are not affected. Since optical excitations start from the VB of Ag_2Se, the barrier can block electrons excited by photons with energy $E < \Delta E + E_g(Ag_2Se) = \Delta E + 0.1$ eV. This explains why the ZnS coating only works for the long wavelengths (1000–2500 nm) and not the short wavelengths (350–1000 nm). For the Ti-iP coated sample, the mechanism is simple. Prior to the Ti-iP coating, photoelectrons can recombine with holes in the electrolyte at the FTO/electrolyte interface (Fig. 7(c)). After the Ti-iP coating, a thin layer of TiO_2 is formed on the FTO surface (Fig. 7(d)). This reduces the contact area between the FTO glass and the electrolyte, hence, recombination is reduced. The process does not involve energy levels of the QDs, consequently, the enhancement does not depend on wavelength.

It is of interest to compare Ag_2Se to the similar system Ag_2S. The advantage of Ag_2Se is the broadband absorption that covers the entire solar spectrum, resulting in high photocurrent densities J_{ph}. The open-circuit voltage ($V_{oc} \sim 0.28$ V) is modest. Since the theoretical upper limit of V_{oc} is equal to $E_{CB}(TiO_2) - E_{redox}$(electrolyte), V_{oc} can be enhanced by using a lower $E_{redox.}$ Hence, the efficiency of Ag_2Se DSSCs may be improved by choosing an electrolyte with a lower redox energy level E_{redox}. For the Ag_2S system, the advantage is that its energy gap of $E_g = 1.1$ eV is equal to the gap for an optimal solar absorber. This gap is the best choice for a solar absorber that can produce the maximal output power. Thus, we expect that both Ag_2S and Ag_2Se systems have the potential for higher efficiencies in the future.

4. Conclusions

In summary, we have successfully fabricated Ag_2Se solar cells by the SILAR of QDs on nanoporous TiO_2 electrodes. The EQE spectrum covers the entire solar power spectrum with a high average EQE. The solar cells yield high current densities, an efficiency of ~3.1% under 9.7% sun, and have the potential for higher efficiencies.

Acknowledgment

The authors are grateful to the financial support received from the National Science Council of the Republic of China.

Appendix A. Supplementary data

Supplementary data associated with this article can be found, in the online version, at doi:10.1016/j.jpowsour.2011.03.074.

References

[1] M.K. Nazeeruddin, F.D. Angelis, S. Fantacci, A. Selloin, G. Viscardi, P. Liska, S. Ito, B. Takeru, M. Grätzel, J. Am. Chem. Soc. 127 (2005) 16835–16847.
[2] Y. Itzhaik, O. Niitsoo, M. Page, G. Hodes, J. Phys. Chem. C 113 (2009) 4254–4256.
[3] A. Belaidi, T. Dittrich, D. Kieven, J. Tornow, K. Schwarzburg, M. Lux-Steiner, Phys. Status Solidi (RRL) 2 (2008) 172–174.
[4] W.W. Yu, X. Peng, Angew. Chem. Int. Ed. 41 (2002) 2368–2371.

[5] I. Moreels, K. Lambert, D.D. Muynck, F. Vanhaecke, D. Poelman, J.C. Martins, G. Allan, Z. Hens, Chem. Mater. 19 (2007) 6101–6106.
[6] R.D. Schaller, V.I. Klimov, Phys. Rev. Lett. 92 (2004), 186601/1–4.
[7] L.M. Peter, D.J. Riley, E.Z. Tull, K.G.U. Wijayantha, Chem. Commun. (Cambridge) (2002) 1030–1031.
[8] I. Robel, V. Subramanian, M. Kuno, P.V. Kamat, J. Am. Chem. Soc. 128 (2006) 2385–2393.
[9] P. Hoyer, R. Könenkamp, Appl. Phys. Lett. 66 (1995) 349–351.
[10] R. Plass, P. Serge, J. Krüger, M. Grätzel, J. Phys. Chem. B 106 (2002) 7578–7580.
[11] A. Tubtimtae, K.L. Wu, H.Y. Tung, M.W. Lee, G.J. Wang, Electrochem. Commun. 12 (2010) 1158–1160.
[12] R. Dalven, R. Gill, Phys. Rev. 159 (1967) 645–649.
[13] Karakaya, W.T. Thompson, Binary Alloy Phase Diagrams, vol. 1, ASM international, Materials Park, OH, 1990, pp. 88–92.
[14] H.M. Pathan, C.D. Lokhande, Bull. Mater. Sci. 27 (2004) 85–111.
[15] V. Buschmann, G.V. Tendeloo, Ph. Monnoyer, J.B. Nagy, Langmuir 14 (1998) 1528–1531.
[16] J.J. Zhao, B.T. Jiang, S.Y. Zhang, H.L. Niu, B.K. Jin, Y.P. Tian, Sci. China Ser. B Chem. 52 (2009) 2213–2218.
[17] G.A. Wiegers, Am. Mineral. 56 (1971) 1882–1888.
[18] Y.L. Lee, C.H. Chang, J. Power Sources 185 (2008) 584–588.
[19] Y.L. Lee, Y.S. Lo, Adv. Funct. Mater. 19 (2009) 604–609.
[20] M. Grätzel, Prog. Photovolt. Res. Appl. 8 (2000) 171–185.